atmosphere

MDPI

Article

Assessing the Impact of Land Use and Land Cover Data Representation on Weather Forecast Quality: A Case Study in Central Mexico

Erika Danaé López-Espinoza [1,*], Jorge Zavala-Hidalgo [1], Rezaul Mahmood [2] and Octavio Gómez-Ramos [3]

1 Centro de Ciencias de la Atmósfera, Universidad Nacional Autónoma de México, Mexico City 04510, Mexico; jzavala@atmosfera.unam.mx
2 High Plains Regional Climate Center, School of Natural Resources, University of Nebraska-Lincoln, Lincoln, KY 68583, USA; rmahmood2@unl.edu
3 Instituto de Geofísica, Universidad Nacional Autónoma de México, Mexico City 04510, Mexico; octavio@geofisica.unam.mx
* Correspondence: danae@atmosfera.unam.mx; Tel.: +52-55-5622-4045

Received: 6 October 2020; Accepted: 23 October 2020; Published: 18 November 2020

Abstract: In atmospheric modeling, an accurate representation of land cover is required because such information impacts water and energy budgets and, consequently, the performance of models in simulating regional climate. This study analyzes the impact of the land cover data on an operational weather forecasting system using the Weather Research and Forecasting (WRF) model for central Mexico, with the aim of improving the quality of the operative forecast. Two experiments were conducted using different land cover datasets: a United States Geological Survey (USGS) map and an updated North American Land Change Monitoring System (NALCMS) map. The experiments were conducted as a daily 120 h forecast for each day of January, April, July, and September of 2012, and the near-surface temperature, wind speed, and hourly precipitation were analyzed. Both experiments were compared with observations from meteorological stations. The statistical analysis of this study showed that wind speed and near-surface temperature prediction may be further improved with the updated and more accurate NALCMS dataset, particularly in the forecast covering 48 to 72 h. The Root Mean Square Error (RMSE) of the average wind speed reached a maximum reduction of up to 1.2 m s^{-1}, whereas for the near-surface temperature there was a reduction of up to 0.6 °C. The RMSE of the average hourly precipitation was very similar between both experiments, however the location of precipitation was modified.

Keywords: operational weather forecasting; WRF model; land cover change

1. Introduction

The rapid expansion of urban areas or urbanization represents one of the most notable human-caused transformations of our planet [1,2]. Urbanization leads to land use and land cover changes (LULCC) and modifies the biogeophysical properties of the land surface, including the albedo, emissivity, soil moisture, and surface roughness length. Modifications in biophysical properties lead to changes in the surface flux, atmospheric circulation, and surface energy budget [3–10]. For example, when the surface energy budget is altered, fluxes in heat, moisture, and momentum within the planetary boundary layer (PBL) are directly affected [8]. Local and regional wind and other climate variables are subsequently affected due to horizontal variations in the turbulent sensible heat flux and PBL depth [8,11–13]. The changes in the physical properties can also impact the thermal inertia/heat capacity of the land surface [14]. The nighttime temperatures are more sensitive to heat capacity.

High water contents in soils, such as from irrigation, can increase the heat capacity, as can highly vegetated areas [10,15]. It has been found that surface temperatures can be 6 °C warmer in city centers compared to surrounding rural areas [16]; this phenomenon is known as urban heat island [17–19]. Urbanization also modifies the location of precipitation [9,19–24].

In the past, research on environmental impacts due to LULCC for Mexico City has been conducted with both observational data and Numerical Weather Prediction (NWP) models [25–31]. Jáuregui [26] studied the changes in temperature, humidity, rainfall, and fog due to LULCC using observational data from northeast Mexico City. In this study, it was shown that downwind (6 km) increased the dry season rainfall as a result of the introduction of new moisture sources (e.g., the construction of artificial lakes), and a 1–3 °C increase in the mean maximum temperature, a 1–2 °C increase in the dew point temperature, an increase in humidity, a decrease in the diurnal temperature range, and a higher frequency of ground fog were also found.

On the other hand, Ochoa et al. [30] used the Weather Research and Forecasting (WRF) model to understand the impacts of urbanization, and found that precipitation increased due to decreased urban area and increased forest. They noted that the simulation with increased pollution resulted in a 20–40% decrease in precipitation in the east of Mexico City and a 20% increase in precipitation over mountain areas. They also found that the timing of intense precipitation changed from 1900 to 1600 local time (UTC—6h) due to decreased urbanization (close to pre-LULCC). Studies such as those of López-Espinoza et al. [29] and López-Bravo et al. [31] have analyzed the sensitivity of the WRF model only to changes in the urban cover data and documented an improvement in the weather forecasts. However, these studies were focused on the proper representation of the urban land cover, and limited attention was given to the effect of an accurate representation of other LULC information, such as forest land, agricultural land, rangeland, barren land, etc.

The objective of this study is to evaluate the impacts of the use of different LULC data on simulated meteorological variables (wind speed at 10 m, near-surface temperature at 2 m, and precipitation). In this research, we have used the WRF for central Mexico and improved the operational weather forecasting system capability for central Mexico through the update of the LULC dataset. This work follows those of López-Espinoza et al. [29] and López-Bravo et al. [31] in searching for better forecasts, supporting the decision making in the region.

In this paper, the study area is described in Section 2. The model configuration, the meteorological data, and LULC data are described in Section 3. The results and discussion are presented in Section 4, and the conclusions are in Section 5.

2. Study Area

The study area includes the megalopolis of central Mexico (Figure 1), which covers Mexico City and the States of Puebla, Morelos, Mexico, Hidalgo, Queretaro, and Tlaxcala. Considering the territory of the seven entities, it represents 13.01% of the total area of the country with 33% of the total population. It is the most important industrial and economic region of the country and constitutes one of the largest concentrations of population in Latin America. It is a particularly vulnerable region for hydrometeorological extreme events. It has an average elevation of between 1169 and 2605 m above sea level, with important mountain ranges and volcanoes [32]. The climate in the study area is influenced by its complex orography, as well as by the human modified landscape. Currently, five types of climates influence the area. These are mainly temperate sub-humid and humid in the center of the study area, arid and semi-arid in the southeast and northwest, warm sub-humid in the south, and temperate humid and warm humid in the northwest (Figure 1) (https://www.inegi.org.mx/temas/climatologia/).

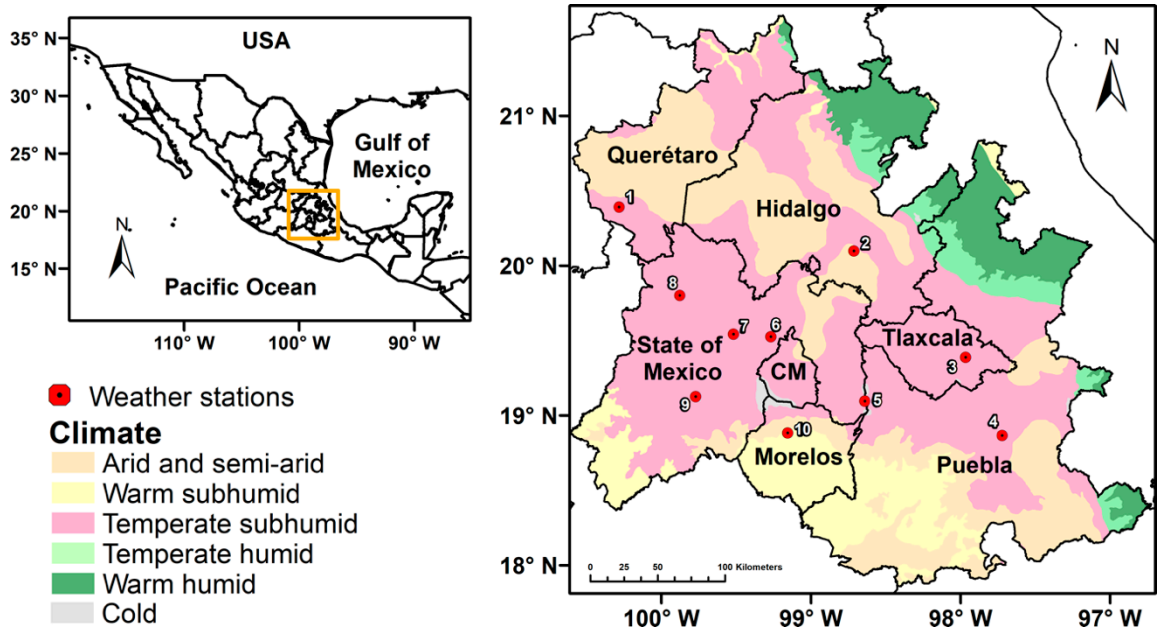

Figure 1. Study area and location of meteorological stations (red circles) used for the evaluation; the colors represent the types of climates that predominate the area.

The average annual rainfall is between 560 to 1270 mm, with most of it May and October (https://worldweather.wmo.int/179/m179.htm). The average annual temperature is between 14 and 22 °C, with 10 and 12 °C in the mountain ranges and volcanoes. In the beginning of the 20th century, the predominant types of land cover were grasslands, shrubland, cropland, and uninhabited arid land. Urban area growth and, in general, the LULC transformations in the seven entities have modified the landscape, and it presents not only a social and political but also an environmental challenge.

3. Methods and Data

3.1. Model Configuration

The WRF model was used to study LULC data quality and its impacts on simulated meteorological variables in an operational weather forecast for central Mexico. Two numerical experiments were completed, one using USGS data [33] (hereafter named the USGS experiment) and another using an updated dataset named the 2005 North American Land Change Monitoring System (NALCMS) [34] (hereafter named the NALCMS experiment).

For the USGS experiment, historical meteorological outputs were used from a weather forecast at the Atmospheric Sciences Center of the National Autonomous University of Mexico (http://grupo-ioa.atmosfera.unam.mx/historicos/). This study applied version 3.6 of the WRF model and used the ARW (Advanced Research WRF) core to solve atmospheric dynamics. The experiment adopted a nesting that covers the megalopolis of central Mexico and its surroundings (Figure 2), with a grid of 205 points from west to east and 124 points from south to north. The nested and parent domains have a horizontal resolution of 6.67 and 20 km, respectively. The domains have 30 vertical levels; the nested domain interacts with the parent domain (one-way nested) and the latter covers the entirety of Mexico. The weather forecast-produced outputs for 5 days and every hour were saved (a 120 h forecast). The initial and boundary conditions were taken from the Global Forecast System (GFS) model with a one-degree spatial resolution. The 0000 UTC data were used for the initial conditions and the boundary conditions every six hours. We used a Mercator projection, a time step of 120 s, and LULC data generated by the USGS in 1992–1993 with 24 classes. The horizontal resolution of the

static geographic dataset used was 10 arc minutes for the 20 km domain and 2 arc minutes for the 6.67 km domain.

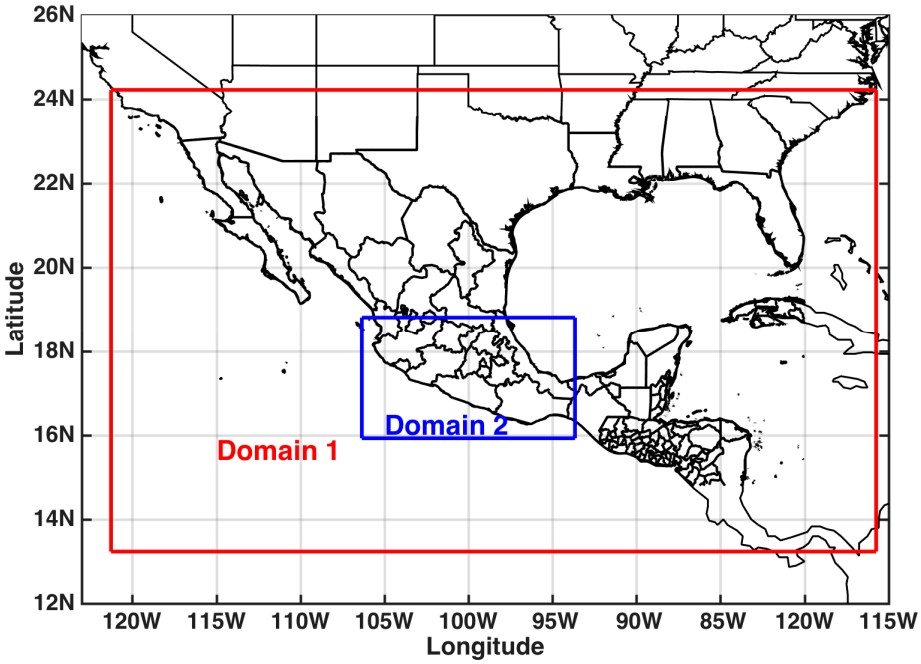

Figure 2. Domains of the numerical experiments. The father domain or Domain 1 (red) has a 20 km horizontal resolution with 245 × 162 grid points, and the nested domain or Domain 2 (blue) has a 6.7 km horizontal resolution with 205 × 124 grid points. The study area is located within Domain 2.

The operational forecast adopted the following physical parameterizations: the Kain–Fritsch scheme for cumulus [35], the single-moment 3-class scheme for microphysics, the Rapid Radiative Transfer Model (RRTM) scheme for longwave radiation, the Dudhia scheme for shortwave radiation, and the Yonsei University (YSU) scheme for the boundary layer [36]. In addition, a 5-layer thermal diffusion scheme [37] was used for the Land Surface Model (LSM). This scheme, although simple, is adequate for mesoscale studies. It is important to consider the fact that this LSM does not predict soil moisture and currently is used more in studies that analyze the performance of LSMs for different regions [38–40]. These studies have indicated that the selection of an LSM can notably affect the simulation results [39,40]; however, their performances (LSMs such as Noah, Pleim–Xiu, Rapid Update Cycle (RUC), Thermal Diffusion) have been reasonably good for the prediction of the near-surface temperature at 2 m and the wind speed at 10 m [38–40], but not for the relative humidity, where the errors have been found to be significant [40]. In particular, the Thermal Diffusion scheme has been found to overestimate (underestimated) the sensible heat (latent heat) flux during the daytime [40]. Taking this into consideration, the scope of this study was limited to analyzing the impact of LULC data quality for predicting meteorological variables for Mexico, rather than considering evaluating aspects of LSM performance.

3.2. Description and Assessment of the Experiments

The NALCMS experiment used the same configuration and physical parameters described above but with a different LULC dataset. Each experiment, USGS and NALCMS, considered a period of two dry months (January and April of 2012) and two rainy months (July and September of 2012). These months are representative of climatic conditions in the study area, which is characterized by two well-defined seasons: the dry season, which spans from November to April, and the rainy season, which is from May to October. A 120 h forecast was run for each day of the 4 months and, in total, 122 numerical simulations were carried out in each experiment (244 in total). The analysis was carried

out every 24 h: 1–24, 25–48, 49–72, 73–96, and 97–120 h. In other words, the first 24 h simulated of each day of the month were analyzed in order to obtain the behavior of 1–24 h, then the following 48 simulated hours of each day were analyzed to obtain the behavior of the next 48 h (25–48 h), and so on up to the 120 h forecast (97–120 h).

The accuracy of the weather forecast was analyzed for the near-surface temperature at 2 m, the wind speed at 10 m, and the hourly precipitation. An assessment of the reliability of both experiments was completed by comparing them with observations from meteorological stations located in the study area (Figure 1). The assessment was performed using the Root Mean Square Error (RMSE) and the Mean Absolute Error (MAE) [41]. The RMSE is a quadratic scoring rule which measures the average magnitude of the error (Equation (1)). The MAE measures the average magnitude of the errors in a set of predictions, without considering their sign (Equation (2)). The difference between them is that MAE is a linear score, which means that all the individual differences are weighted equally in the average, while RMSE gives a relatively high weight to large errors. For both the MAE and RMSE, lower values represent a better agreement.

$$RMSE = \sqrt{\frac{\sum_{i=1}^{n}(s_i - o_i)^2}{n}}, \quad (1)$$

$$MAE = \frac{\sum_{i=1}^{n}|s_i - o_i|}{n}, \quad (2)$$

where S_i is the predicted variable, O_i is the observation, and n is the total number of data.

3.3. Meteorological Data

Meteorological stations (Estaciones Meteorológicas Automáticas—EMA for its Spanish acronym) from the Mexico's National Weather Service (Servicio Meteorológico Nacional—SMN for its Spanish acronym) were used to assess the experiments. Although SMN is the Mexican agency responsible for providing meteorological information, a visual analysis was performed to verify that there were no inaccurate values. Furthermore, the annual percentage of existing data for each EMA station was estimated, and to consider a station a percentage of data equal to or greater than 96% was used as a limit, for which ten stations were selected (Figure 1). EMA stations are available with a temporal frequency of 10 min. A comparison between the predicted and observed values was made, taking into account the nearest grid cell to the meteorological station. The values of each hour were compared for the near-surface temperature (°C) and wind speed (m s^{-1}). The hourly (mm h^{-1}) accumulated observed precipitation was calculated to enable comparison with the simulation results.

3.4. LULC Dataset

The NALCMS dataset was selected to carry out the second experiment (Table 1). The selection was based on the analysis conducted by López-Espinoza et al. [42]. This dataset is a product of a the collaborative effort of governmental agencies from Canada, Mexico, and the United States, coordinated by the North American Environmental Atlas of the Commission for Environmental Cooperation. For this dataset, 2005 Moderate Resolution Imaging Spectroradiometer (MODIS) data at a spatial resolution of 250 m were used. Nineteen land cover classes were defined using the Land Cover Classification System (LCCS) [43]. To generate the final dataset, each country used their own training data and classification methods, and the final dataset was a combination of the datasets generated by the three countries. For Mexico, the inputs were the monthly composite of the MODIS radiance data, the Normalized Difference Vegetation Index (NDVI) data, and information from a Digital Elevation Model. NALCMS has a successor developed in 2010; however, previous studies have demonstrated that this dataset does not present significant land cover changes in the simulated nested domain (Figure 2, Domain 2), and even less in our study area [44,45].

Table 1. Comparison of the main characteristics of the USGS and NALCMS LULC data used in the experiments.

	USGS	NALCMS
Sensor	AVHRR	MODIS
Period of data collection	April 1992–March 1993	January 2005–December 2005
Processing	By continent	3 regions
Input data	Monthly NDVI compositions	Different data by country
Spatial resolution	1 km	250 m
Classification strategy	Unsupervised based on grouping	Supervised with threes C5 (for Mexico)
Legend system	24 USGS	19 LCCS-FAO
Developers	USGS-IGBP	CCRS, USGS, INEGI, CONABIO, CONAFOR

On the other hand, studies have shown that the USGS dataset has a low classification accuracy [3,6,14,29], and in atmospheric modeling an accurate representation of LULC is desirable because such information impacts the water and energy budgets, and, consequently, the performance of models in simulating regional climate.

A pre-processing of the data was required in order to convert the NALCMS into the same coordinate, spatial resolution, and classification scheme of the USGS [42]. In the pre-processing step, the dataset was converted into a latitude-longitude coordinate system using a 1 km spatial resolution. To standardize the NALCMS classes, each legend was related to the most suitable USGS class. The USGS classification scheme is defined with 24 classes, and it is based on Anderson's classification scheme [46] (first column in Table 2). However, only the 11 classes shown in Table 2 are present in the study area. On the other hand, NALCMS is defined with 19 land cover classes, of which 13 are present in the study area. The standardization was achieved based on the best available information reported in regional maps and the literature about the continental and global scale datasets [47–49]. Table 2 shows the reclassification of the NALCMS dataset to the USGS class scheme. The dryland cropland/pasture and irrigated cropland/pasture classes of USGS are grouped into a class called cropland in the NALCMS dataset. The moisture and energy budgets of irrigated cropland are different from those of dry cropland. However, due to uncertainty in the irrigation/pasture cropland data and the potentially smaller total area of irrigated croplands, the cropland class is used as a compromise (Figure 3).

Table 2. Translation from the NALCMS to the USGS classification scheme.

Anderson's Classification Scheme	USGS	NALCMS
Urban	Urban and built up land	Urban and built-up
Agricultural land	Dryland cropland/pasture	Cropland
	Irrigated cropland/pasture	
Rangeland	Grassland	Tropical or sub-tropical grassland
		Temperate or sub-polar grassland
	Shrubland	Tropical or sub-tropical shrubland
		Temperate or sub-polar shrubland
Forest	Deciduous broadleaf forest	Tropical or sub-tropical broadleaf deciduous forest
		Temperate or sub-polar broadleaf deciduous forest
	Evergreen broadleaf forest	Tropical or sub-tropical broadleaf evergreen forest
	Evergreen needleleaf forest	Temperate or sub-polar needleleaf evergreen forest
	Mixed forest	Mixed forest
Water	Water bodies	Water
Barren land	Barren or sparsely vegetated	Barren land

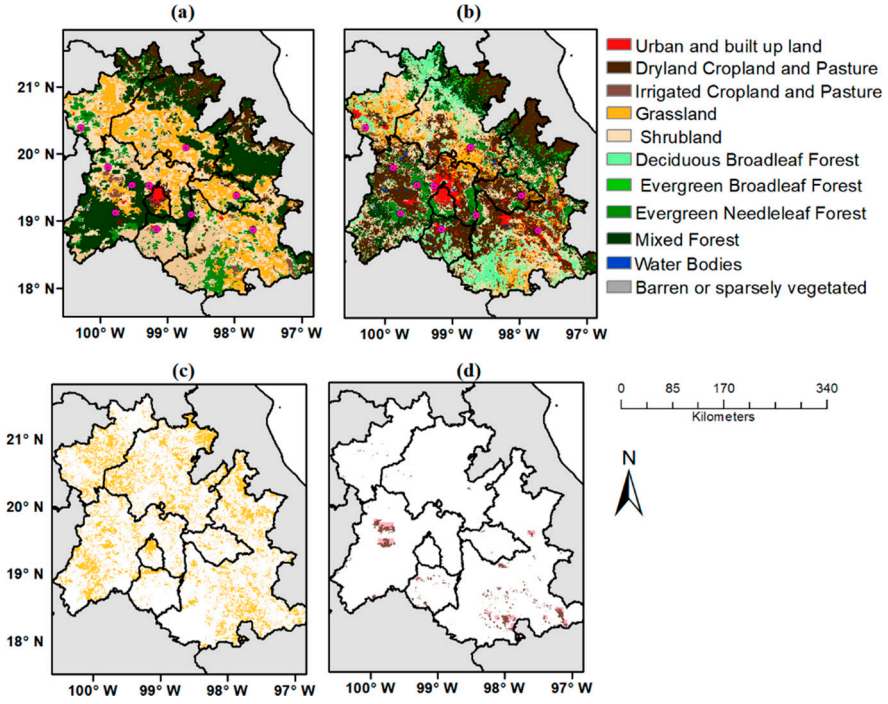

Figure 3. LULC datasets for the study area: (**a**) USGS, (**b**) NALCMS. Pink circles represent location of meteorological stations. (**c**) White represents the areas that changed from 1993 to 2005, yellow represents the areas that do not show LULC changes, (**d**) brown represents the dryland cropland class with a 250 m resolution, and pink represents the same class at a 6.667 km resolution.

Changes of LULC

Table S1 (Supplementary Material) shows details about LULCC by means of the estimated change matrix over the entire study area. Figure 3c shows in white the areas that changed (the elements off the diagonal of the matrix), while yellow represents the areas that did not show LULC changes (diagonal of the matrix). Table 3 shows the LULC changes at each meteorological station with 1 km spatial resolution (Domain 2), which are consistent with the observed changes in the original resolution of the NALCMS dataset (250 m). The LULCCs around the selected meteorological stations were characterized mainly by the loss of forest, shrubland, and grassland, and these were replaced by cropland, grassland, and urban and built-up land. The loss of mixed forest is related to the loss of the deciduous forest, leaving only the evergreen forest (stations 5 and 9). The evergreen forest (stations 3 and 4) and shrubland (stations 1, 8, and 10) were converted to cropland for food production. The vegetation cover at station 6 was modified into urban and built-up land. Given these changes in LULC around the different meteorological stations, and in general over the entire study area (Figure 3c in white color and Table S1), changes in the physical properties of the terrain (Table 4) have also occurred and led to changes in the surface flux, atmospheric circulation, and surface energy budget [5].

Table 3. Land cover change at each station. ID represents the location in Figure 1.

ID	Station	USGS	NALCMS
1	Huimilpan, Qro.	Shrubland	Cropland
2	Pachuca, Hgo.	Grassland	Grassland
3	Huamantla, Tlax.	Evergreen Needleleaf Forest	Cropland
4	Universidad Tecnológica de Tecamachalco, Pue.	Evergreen Needleleaf Forest	Cropland
5	Parque-Izta-Popo, Edo. Méx.	Mixed Forest	Evergreen Needleleaf Forest
6	Presa Madín, Edo. Méx.	Shrubland	Urban and Built-Up Land
7	Cerro Catedral, Edo. Méx.	Shrubland	Evergreen Needleleaf Forest
8	Atlacomulco, Edo. Méx.	Shrubland	Cropland
9	Nevado de Toluca, Edo. Méx.	Mixed Forest	Evergreen Needleleaf Forest
10	Instituto Mexicano de Tecnología del Agua, Mor.	Shrubland	Cropland

Table 4. Parameters associated with each type of cover land (see file LANDUSE.TBL of the WRF model). Sum: summer; values from 15 April to 15 October, Win: winter; values from 15 October to 15 April.

Land Cover Category	Albedo (%) [ALBEDO]		Roughness Length (m) [SFZ0]		Emissivity (% at 9 μ m) [SFEM]	
	Sum	Win	Sum	Win	Sum	Win
Urban and Built-Up Land	15	15	0.80	0.80	88	88
Dryland Cropland and Pasture	17	23	0.15	0.05	98.5	92
Irrigated Cropland and Pasture	18	23	0.15	0.05	98.5	92
Grassland	19	23	0.12	0.10	98.5	92
Shrubland	22	25	0.10	0.10	88	88
Evergreen Needleleaf Forest	12	12	0.50	0.50	95	95
Mixed Forest	13	14	0.50	0.50	94	94

4. Results and Discussion

4.1. Near Surface Temperature

Maps of the monthly average temperature are shown in Figure S1 (Supplementary Material). The absolute difference was calculated between the NALCMS and USGS experiments. The highest absolute difference was about 0.5–1 °C for the regions with conversion from vegetation to urban land. It was also found that the absolute difference in the average daily maximum temperature (Supplementary Material, Figure S2) can reach up to 2.5 °C, mainly in the regions around the newly urbanized centers and in the regions where there was a conversion from shrubland to cropland and urban land. Maps of the monthly average daily minimum temperature (Supplementary Material, Figure S3) showed absolute differences between 0.5 to 2 °C for the dry months, and values between 0.5 to 1.5 °C for the rainy months. These results are consistent with those of previous studies of the thermal behavior of urban land compared to vegetated land [17,18], where the largest near-surface temperature differences are observed during noon.

Figure 4 shows the time series for the monthly average surface temperature for station 6 in January. It can be seen that there was an increase in the daily maximum temperature [7,50] and a decrease in the daily minimum temperature using updated data [17]. This was due to the new urban areas represented in the NALCMS data, where values close to observations were predicted. Replacing shrubland with

urban and built-up land reduced the albedo from 25 to 15, and this improved the forecast of the near-surface temperature. Additionally, the shrubland has a higher albedo and emissivity than urban and built-up land, and hence its temperature during the day was lower than that of urban land. In addition, during the night the highest minimum temperature was estimated. These results are consistent with the measured surface temperature profiles by Shamsipour et al. [17].

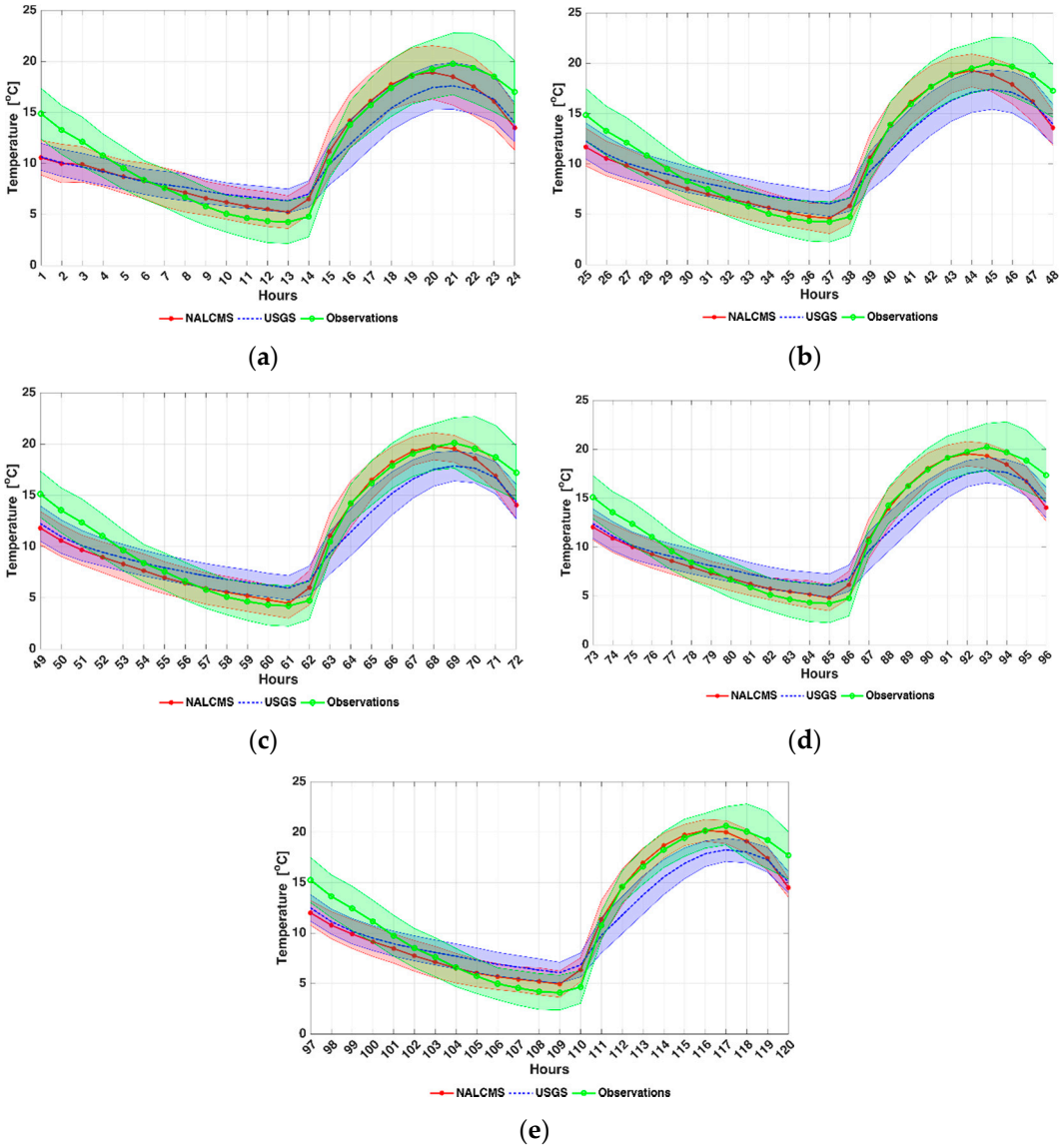

Figure 4. Time series of station 6 in the State of Mexico for the near-surface temperature during the 120 h forecast for January 2012. The horizontal axis corresponds to the hours and the vertical axis corresponds to the temperature in degrees Celsius. The thick lines (—,-*-,-o-) represent the monthly average and the shaded area represents one standard deviation. Green (-o-) represents the average of observations, red (-*-) represents the average of the experiment using the NALCMS data, and blue (—) represents the average of the experiment using the USGS data. (**a**) 24 h forecast, (**b**) 48 h forecast, (**c**) 72 h forecast, (**d**) 96 h forecast, and (**e**) 120 h forecast.

The RMSE was calculated by comparing the observed and predicted near-surface temperature values. Figure 5 shows the RMSE for the monthly average of the surface temperature for the 10 stations during the 120 h of forecast. For January (dry month) and in the 72–96–120 h forecast (Figure 5a), it is observed that the minimum value of RMSE (lower whisker), together with 25% of the data, or the first

quartile Q_1, was reduced when the NALCMS data was used. For the same month, a RMSE reduction was not observed if more than 50% of the data, or the second quartile Q_2, is considered. For April (dry month), an increase in the RMSE values was observed when using the NALCMS data. In the rainy months (Figure 5c,d), the minimum values of RMSE (lower whisker) were reduced for the NALCMS data. For this month (July), after 24 h of forecast 75% of the data (Q_3) resulted in a smaller RMSE when using the NALCMS. Like April, the month of September did not produce lower errors when using the NALCMS. Finally, in both rainy months, outliers with lower RMSE values were observed when using the updated LULC.

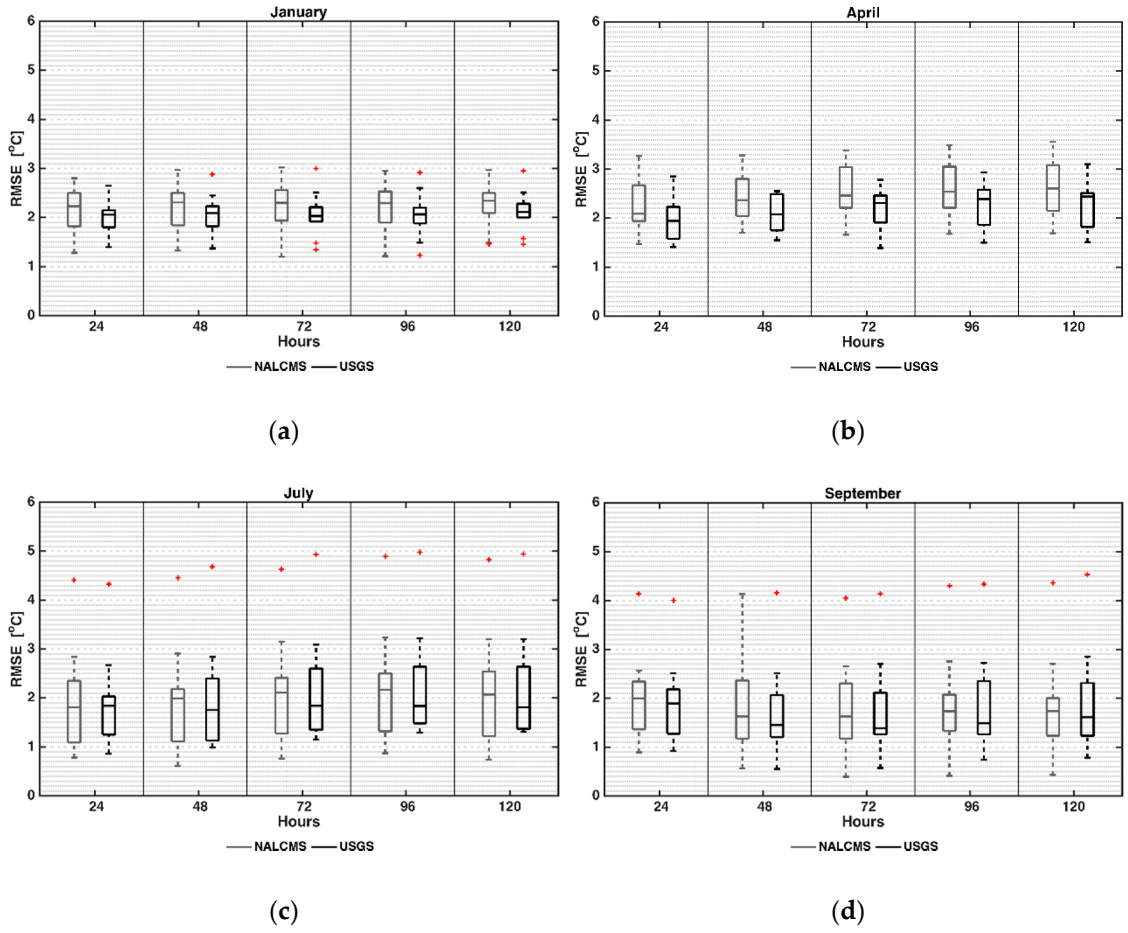

Figure 5. RMSE between the predicted and observed values for the monthly average of the daily temperature of the 10 stations during the 120 h of forecast. The horizontal axis corresponds to the forecast hours and the vertical axis corresponds to the RMSE in degrees Celsius. Gray boxes represent the NALCMS RMSE and black boxes represent the USGS RMSE for (**a**) January, (**b**) April, (**c**) July, and (**d**) September.

Using the updated NALCMS data, the RMSE of the predicted near-surface temperature was reduced up to 0.6 °C for July (rainy month) compared to the USGS data. This is observed for a 48 h forecast (Figure 5). The maximum reduction in RMSE was reached at station 3, where the LULC changed from evergreen needleleaf forest to cropland. The changes in land cover caused modifications in the vegetation and in the physical properties of the terrain such as albedo (from 12% to 18% for station 3), which modified the near-surface temperature as well as the daily maximum and minimum temperature extremes. Albedo together with emissivity (from 95% to 88% for station 3) impacted the upwelling of longwave radiation (not shown) [5,8]. Similar results were found at station 10, where the conversion from shrubland to cropland had a reduction in RMSE of up to 0.5 °C; station 7, where the

conversion from shrubland to evergreen needleleaf forest had a reduction of up to 0.3 °C; and at station 8, with conversion from shrubland to cropland, where a reduction of 0.2 °C was obtained. In the other stations, when NALCMS was used, the reduction in RMSE was less. For September, a similar behavior was observed from the 96 h forecast, and for January (dry month) the RMSE reduction in temperature was observed only in three meteorological stations (1, 6, and 7). However, these smallest RMSE values were observed for the entire five-day forecast.

Figure 6 shows the RMSE and MAE of the daily maximum and minimum temperature from the 10-station average for the dry and rainy seasons. The RMSE values were reduced for the rainy season (July and September) (Figure 6b), principally after the 72 h forecast. For the dry season, a decrease in the MAE was observed for January during the entire five-day forecast (Figure 6a); however, for April there was no improvement in the predicted maximum temperature when the NALCMS data were used. Finally, only in January (dry month) was there a reduction in the MAE values for the predicted minimum temperature, particularly for the 96 h forecast (Figure 6c).

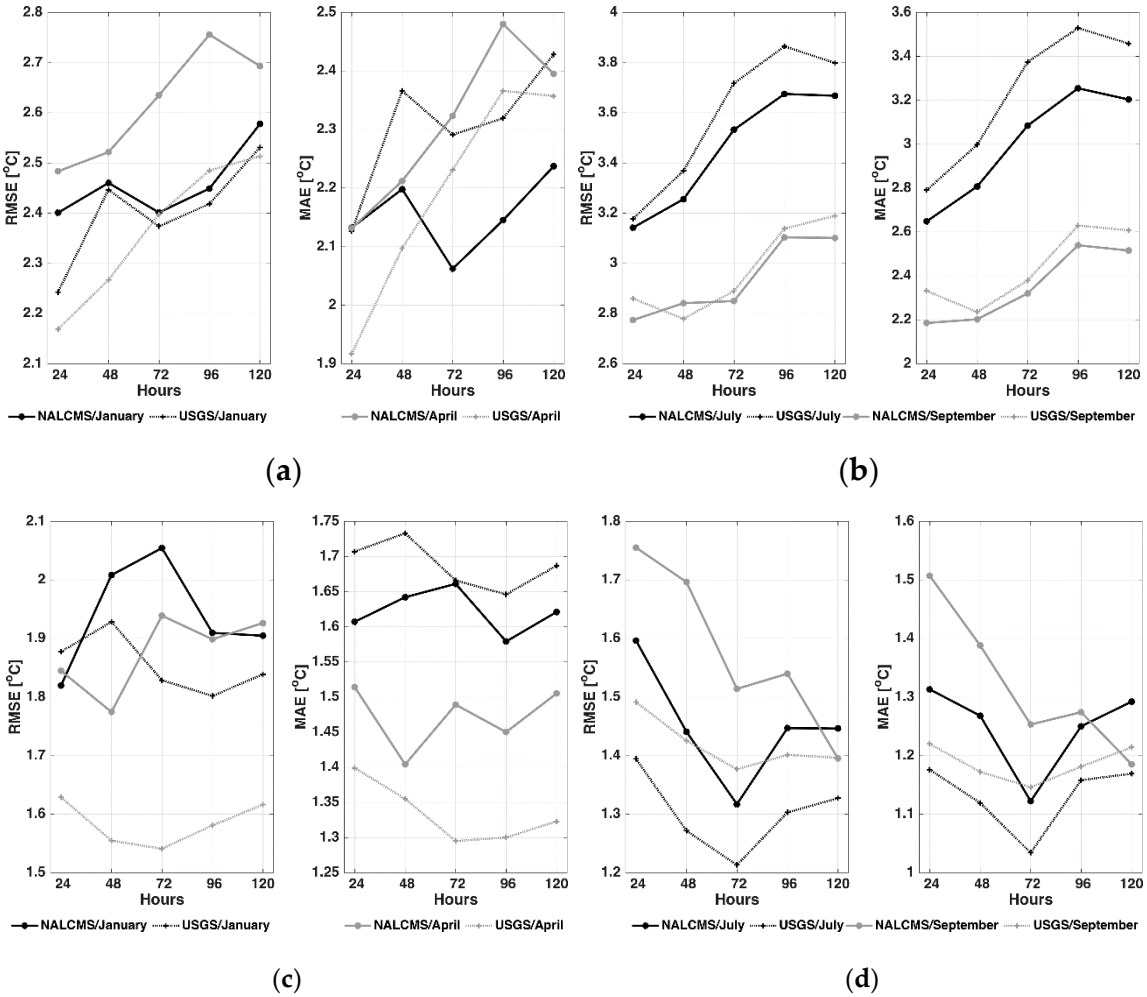

Figure 6. RMSE and MAE for the stations during the 120 h of forecast. The horizontal axis corresponds to the forecast hours and the vertical axis corresponds to the RMSE or MAE in degrees Celsius. Solid black and gray lines represent the NALCMS experiment, and black and gray dotted lines represent the USGS results. Average daily maximum temperature: (**a**) dry season (January and April), (**b**) rainy season (July and September). Average daily minimum temperature: (**c**) dry season (January and April), (**d**) rainy season (July and September).

4.2. Wind Speed

Difference maps for the monthly average maximum and minimum wind speed between the NALCMS and USGS experiments are shown in Figures S4 and S5 (Supplementary Material). It was found that the daily maximum and minimum wind speed using the USGS data were higher than using the NALCMS data, and that higher wind speeds occurred in surfaces with lower friction (USGS) and were lower where there was urban and forest land (NALCMS). Changes in the surface roughness (Table 4) due to land cover changes impacted the wind speed during the entire five-day forecast.

In Figure 7, the time series of the predicted and observed wind speed are shown for station 6 in April. At this location, the land cover changed from shrub to urban land, which led to changes in the surface roughness length from 0.10 to 0.80 (Table 4); as a consequence, the overestimation of the wind speed was reduced when NALCMS was used. The friction and drag of the updated land cover with greater roughness around stations 1, 8, 10, 4, 6, and 7, decreased the wind speed, with an average RMSE of up to 0.6 m s^{-1} in January (Figure 8a), 0.5 m s^{-1} in September (Figure 8d), and 0.4 m s^{-1} in April and July (Figure 8b,c). The maximum reduction in RMSE reached when NALCMS was used was up to 1.1 m s^{-1} in January (stations 1 and 4), 0.8 m s^{-1} in April (station 1), 1.2 m s^{-1} in July (station 4), and 0.9 m s^{-1} in September (station 4). This reduction was observed from a 48 h forecast.

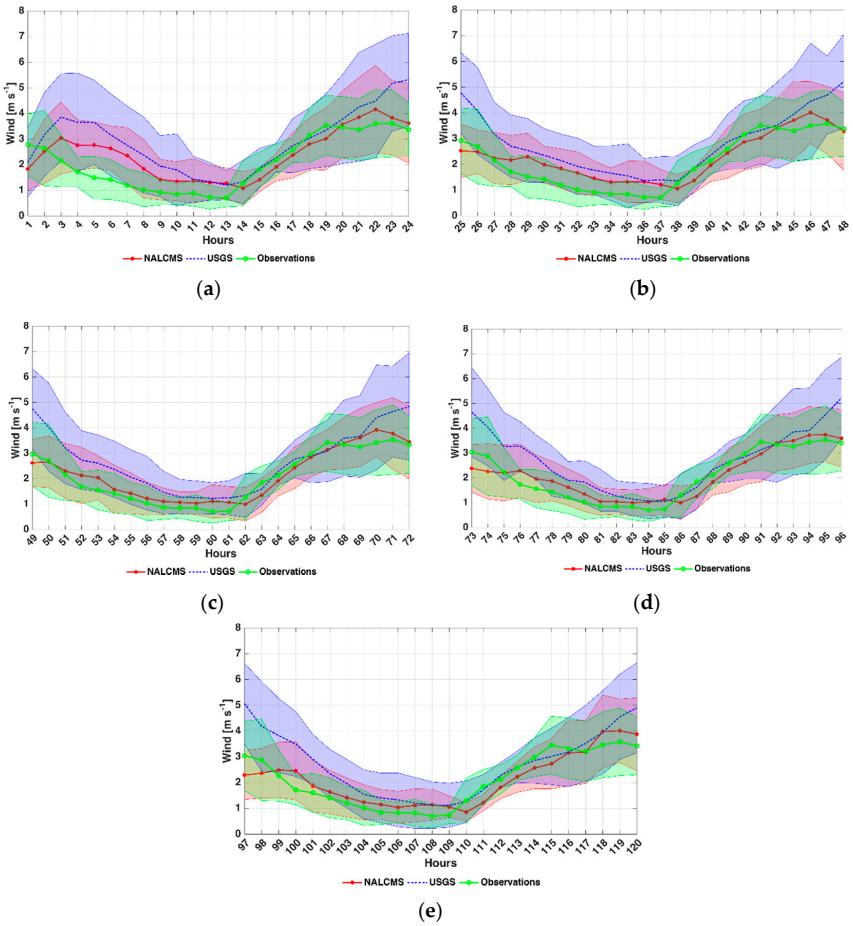

Figure 7. Time series for station 6 in the State of Mexico for the wind speed at 10 m during the 120 h forecast. The horizontal axis corresponds to the simulated hours and the vertical axis corresponds to the wind speed in m s^{-1}. The thick lines (—,-*-,-o-) represent the monthly average and the shaded area represents one standard deviation. -o- (green line) represents the average of observations, -*- or red line (— or blue line) represents the average of the experiment using the NALCMS (USGS) data. (**a**) 24 h forecast, (**b**) 48 h forecast, (**c**) 72 h forecast, (**d**) 96 h forecast, and (**e**) 120 h forecast.

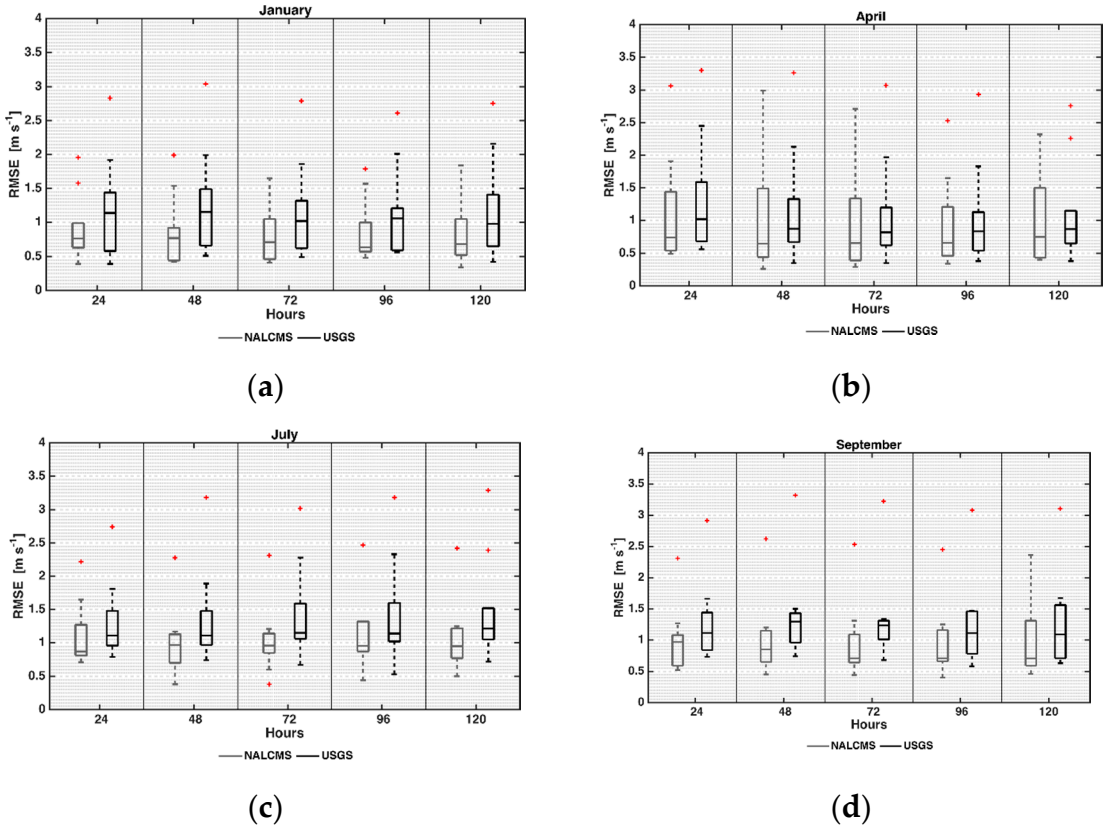

Figure 8. RMSE between the model and observations of the average monthly wind speed at 10 m for the 10 stations during the forecast of 120 h. The horizontal axis corresponds to the simulated hours and the vertical axis corresponds to the RMSE in m s^{-1}. Gray color boxes represent the NALCMS RMSE and black color boxes represent the USGS RMSE. (**a**) January, (**b**) April, (**c**) July, and (**d**) September.

Figure 9 shows the RMSE and MAE of the average daily maximum and minimum wind speed of the 10 stations during the dry and rainy season. When the NALCMS was used instead of USGS, the RMSE values for maximum (minimum) wind speed were reduced up to 0.39 m s^{-1} (0.45 m s^{-1}) in January and up to 0.11 m s^{-1} (0.19 m s^{-1}) in April. For the rainy season, the RMSE values for the maximum (minimum) wind speed decreased more than those obtained in the dry season: 0.55 m s^{-1} (0.27 m s^{-1}) in July and 0.52 m s^{-1} (0.28 m s^{-1}) in September. The smallest RMSE occurred between the 72 and 96 h of forecast when the NALCMS was used. Additionally, the MAE values of the average maximum wind speed were reduced more than the MAE of the average minimum wind speed. For the dry season, the MAE values for the maximum (minimum) wind speed were reduced up to 0.53 m s^{-1} (0.36 m s^{-1}), whereas for the rainy season they were reduced up to 0.46 m s^{-1} (0.25 m s^{-1}). The errors for the maximum wind speed occurred between 48 and 96 h of the forecast (Figure 9a,b), while for the minimum wind speed they were observed from 24 to 96 h of the forecast (Figure 9c,d).

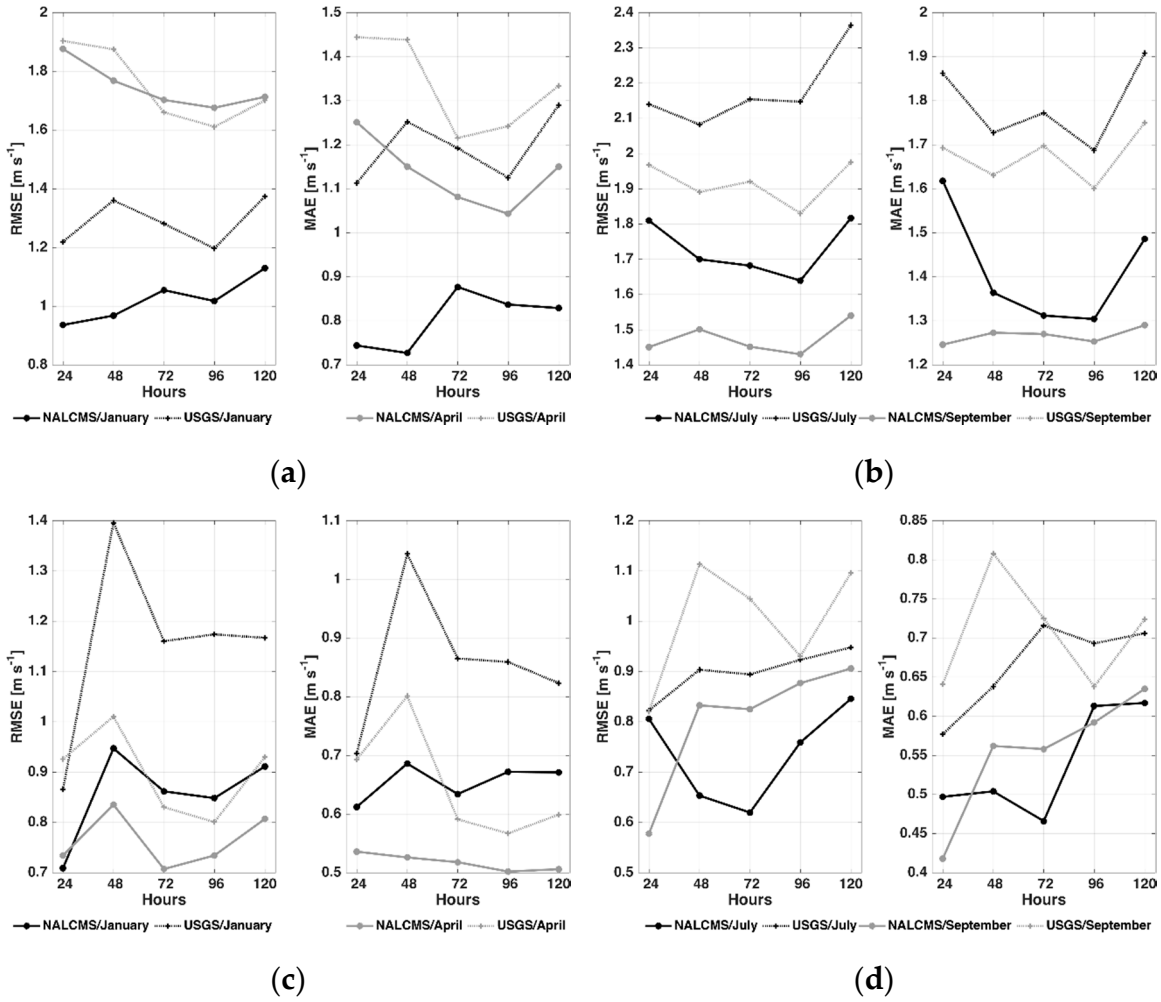

Figure 9. RMSE and MAE of the average maximum and minimum wind speed for the 10 stations during the 120 forecast hours. The horizontal axis corresponds to the simulated hours and the vertical axis corresponds to the RMSE or MAE in m s^{-1}. Solid black and gray lines represent the NALCMS experiment, and the black and gray dotted lines represent the USGS experiment. Average maximum wind speed: (**a**) dry season (January and April), (**b**) rainy season (July and September); average minimum wind speed: (**c**) dry season (January and April), (**d**) rainy season (July and September).

4.3. Precipitation

Maps of the average daily accumulated precipitation are shown in Figure S6 (Supplementary Material). Analysis suggests that, for the dry months, both experiments produced a similar spatial distribution of the precipitation. On the other hand, for the rainy months during the 48 h forecast, the maximum increase was up to 19 mm d^{-1} when the NALCMS was used. This was observed mainly in the center (Mexico City) and west (State of Mexico) of the study area (Figure 1). The average hourly precipitation rate (Supplementary Material, Figure S6) did not change significantly for the dry months, and the WRF model correctly predicted the absence of precipitation with either of the two LULCs. For this reason, the analysis was focused on rainy months, which it was observed that the location of precipitation was modified [20–24].

In Figure 10, the predicted and observed average hourly precipitation is shown for station 10 for September. At this location, the conversion from shrubland (USGS) to dryland cropland (NALCMS) decreased the amount of latent heat flux (not shown), which led to a decrease in precipitation. With these results, predicted values closer to the observations were obtained, however this did not happen for all stations.

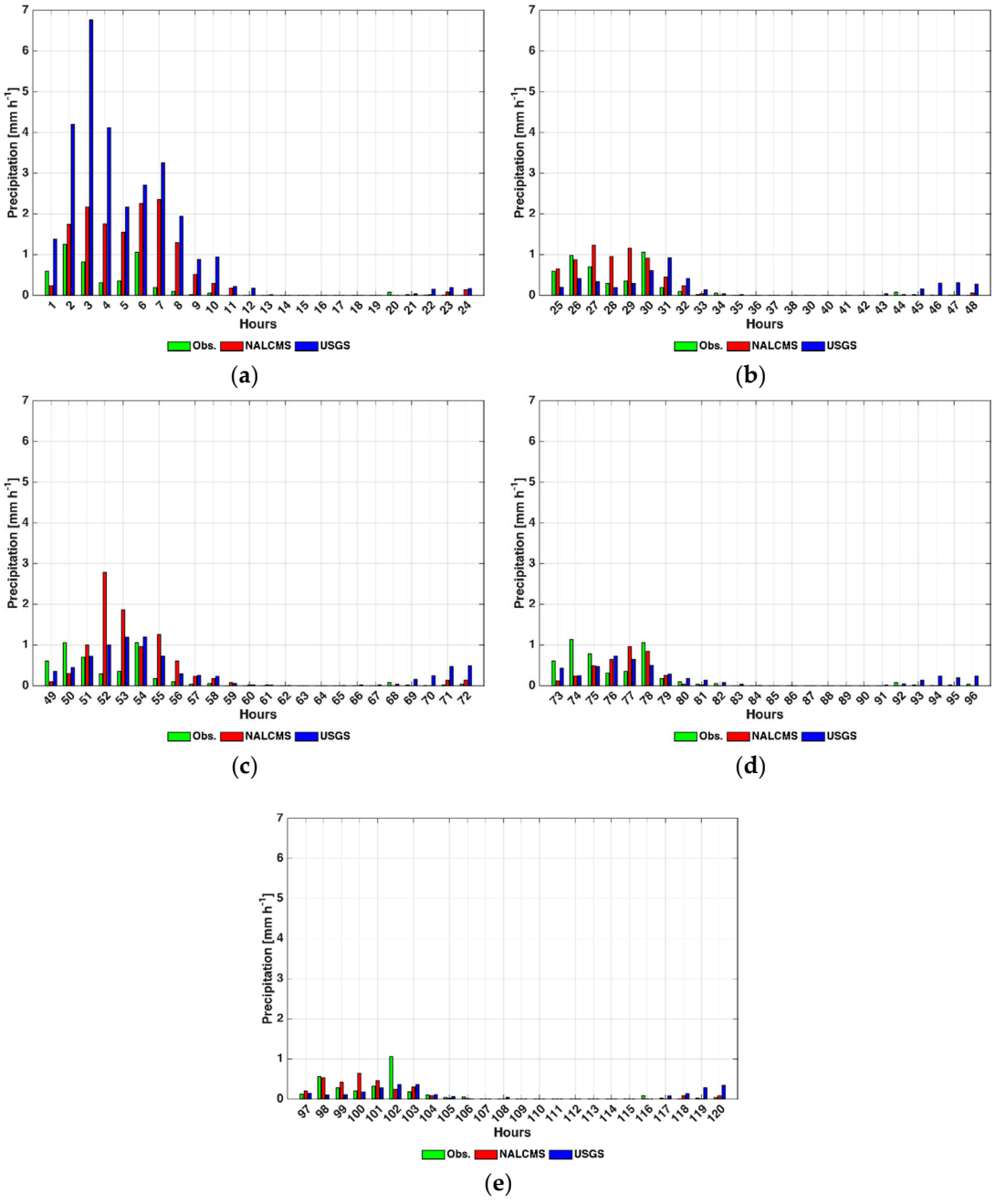

Figure 10. Average hourly precipitation for station 10 in the State of Mexico during the 120 h Figure 1. The thick bars represent the monthly average. Green bar represents the average of observations, and the red (blue) bar the average of the experiment using the NALCMS (USGS) data. (**a**) 24 h forecast, (**b**) 48 h forecast, (**c**) 72 h forecast, (**d**) 96 h forecast, and (**e**) 120 h forecast.

The RMSE was calculated for the hourly precipitation during the 120 h of forecast. Table 5 shows the maximum RMSE values for the 10 stations. Using the NALCMS (USGS) data, the maximum RMSE values are between 0.73 (0.38) and 1.24 (1.15) mm h^{-1} for July, and between 0.77 (0.41) and 1.56 (0.84) mm h^{-1} for September. It was found that both experiments overestimated the average hourly precipitation; however, the smallest RMSE values were obtained for the USGS data. This is observed in the 120 h forecast in July for both datasets (USGS and NALCMS) and in September in the 48 h forecast for USGS, and during the 96 h forecast for NALCMS (Table 5).

Table 5. Maximum RMSE values reached considering the 10 meteorological stations for the average hourly precipitation during the forecast of 120 h.

		Hourly Precipitation [mm h^{-1}]				
		24-h	**48-h**	**72-h**	**96-h**	**120-h**
July	**NALCMS**	<1.13	<1.24	<1.04	<0.96	<0.73
	USGS	<0.78	<0.60	<1.15	<0.59	<0.38
September	**NALCMS**	<1.42	<1.35	<1.56	<0.77	<1.11
	USGS	<0.77	<0.41	<0.52	<0.79	<0.84

The precipitation results obtained with the NALCMS experiment were very similar to those with USGS. In addition, these results are consistent with those of previous studies, specifically with those of [3,9].

4.4. Physical Processes

Land cover changes have been considered as one of the most significant modifications to natural ecosystems [10]. The improvement in the forecast performance that is observed when using NALCMS is mainly due to the following physical processes.

For temperature, the changes in albedo and sensible and latent heat are the main contributors. Built-up areas alter thermal characteristics and moisture pathways, adding an extra energy supply to the region [1]. The reduction in vegetation and soil in urban areas decreases evapotranspiration and its associated latent heat. This keeps heat in the ground and the daily minimum temperature increases because of the reduction in one of the mechanisms whereby the ground loses heat. The albedo modification produces changes in the amount of energy absorbed (or reflected), affecting the amount of heat exchange between the surface and the atmosphere.

The wind speed predicted by the WRF model is at a height of 10 m and is sensitive to the surface roughness. The wind speed in built-up areas decreases because the height of the urban buildings is usually higher than that of other natural vegetation, which increased the roughness of the surface, hindering the air circulation and lowering the wind speed [11]. In areas where the previous LULC was cropland, urbanization increased friction. On the other hand, in regions where the previous land cover was forest, the friction may decrease, depending on the type of forest and the average building characteristics (e.g., the height of the buildings).

The impacts of LULC changes on precipitation are complex [2]. Modifications in precipitation are more difficult to attribute to a cause, since several spatial scales are involved in the processes that lead to precipitation changes. Urbanization induces a series of complex changes in land surface roughness, soil moisture, and the exchange of water and energy between the land and the atmosphere [15]. These changes can either offset or enhance each other and complicate the spatial patterns of precipitation [19]. In our study, the microclimates may be modified because under urbanization local thermal convection increases and modifies the small-scale circulation patterns. Since the air temperature increases, this may be a contributor to the delay in the peak hour of precipitation. In addition, changes in local circulation also contributed to modifying the spatial distribution of precipitation.

5. Conclusions

This study evaluated the impacts of two LULC datasets on the operational weather forecast using the WRF model in central Mexico. Two experiments were completed as an operational forecast for 120 h, one using the USGS dataset and another using the NALCMS dataset. The updated NALCMS data agree better with the current land use conditions than the USGS data. Land cover such as

grasslands, shrubland, and mixed and evergreen forests in USGS were replaced by cropland and urban and built-up land.

The RMSE and MAE of the average wind speed at 10 m decreased in the NALCMS experiment in comparison to the USGS experiment. Due to the surface roughness length, the NALCMS data improved the wind speed forecast quality. The friction and drag of the updated surfaces reduced the RMSE up to 0.6 m s^{-1}. The maximum reduction in RMSE reached up to 1.2 m s^{-1}. The RMSE of the maximum wind speed was lower than the minimum wind speed, and larger in the rainy than in the dry season. The lowest RMSE values were observed from a 48 h forecast.

The application of updated and accurate LULC data (NALCMS) improved the forecast of the near-surface maximum and minimum temperatures. The RMSE was reduced up to 0.6 °C during the rainy month (July) from a 48 h forecast. However, the differences between the USGS and NALCMS experiments reached up to 2.5 °C (average daily maximum temperature). During the dry and rainy season, the daily maximum temperature was better predicted mainly during the 72 h forecast and when NALCMS was used, and the daily minimum temperature was better predicted for the dry month (January) during the entire forecast.

The predicted precipitation showed that the WRF model was able to capture the main features of the observed precipitation, and the precipitation results obtained with the new NALCMS data were very similar to those obtained with USGS.

The reduction in the error magnitudes of the variables analyzed is consistent with previous studies, specifically with those of [12,13] for the wind speed at 10 m, [12,13] for the near-surface temperature at 2 m, and [3,9] for the precipitation.

From our results, it was observed that the most reliable forecast is the forecast from 48 to 72 h. This window provides the lowest error on which decision-makers could base their conclusions. This study follows those from [29,31] in the search for better weather forecasts in central México, a region influenced by tropical and middle latitude meteorological systems. The results may apply to other large urban areas.

Finally, even if the weather forecast was improved, research on physical parameterization schemes for the region should be conducted, with a focus on LSM schemes to obtain a better representation of land surface processes. LSMs with a higher level of complexity have been shown to improve predictions [51]. For example, studies such as Teklay et al. [9] have shown that Noah/USGS can decrease the RMSE of precipitation up to 1.36 mm d^{-1} compared to Thermal Diffusion/USGS. However, a combination of Noah and new LULC data can further lower bias. Particularly for Mexico, this is an issue that needs to be investigated in the future.

Supplementary Materials: The following are available online at http://doi.org/10.5281/zenodo.4067211: Table S1, Figures S1–S7.

Author Contributions: Conceptualization, E.D.L.-E.; Data curation, E.D.L.-E. and O.G.-R.; Formal analysis, E.D.L.-E., J.Z.-H., R.M. and O.G.-R.; Funding acquisition, E.D.L.-E. and R.M.; Methodology, E.D.L.-E. and J.Z.-H.; Resources, E.D.L.-E. and J.Z.-H.; Software, E.D.L.-E.; Supervision, E.D.L.-E., J.Z.-H., R.M. and O.G.-R.; Validation, E.D.L.-E.; Writing—original draft, E.D.L.-E. and O.G.-R.; Writing—review and editing, E.D.L.-E., J.Z.-H., R.M. and O.G.-R. All authors have read and agreed to the published version of the manuscript.

Funding: This research was funded by Universidad Nacional Autónoma de México—Dirección General de Asuntos del Personal Académico IT102120; Rezaul Mahmood received support from an NSF Grant AGS-1853390.

Acknowledgments: We would like to thank Comisión General del Servicio Meteorológico Nacional (CGSMN) of the Comisión Nacional del Agua (CONAGUA) for providing us with the observational data.

Conflicts of Interest: The authors declare no conflict of interest.

References

1. Grimmond, S. Urbanization and global environmental change: Local effects of urban warming. *Geogr. J.* **2007**, *173*, 83–88. [CrossRef]
2. Mahmood, R.; Quintanar, A.; Conner, G.; Leeper, R.; Dobler, S.; Pielke, R.; Syktus, J. Impacts of land use/land cover change on climate and future research priorities. *Bull. Am. Meteor. Soc.* **2010**, *91*, 37e46. [CrossRef]
3. Sertel, E.; Robock, A.; Ormeci, C. Impacts of land cover data quality on regional climate simulations. *Int. J. Climatol.* **2010**, *30*, 1942–1953. [CrossRef]
4. Pielke, R.; Pitman, A.; Niyogi, D.; Mahmood, R.; McApline, C.; Hossain, F.; Goldewijk, K.K.; Nair, U.; Betts, R.; Fall, S.; et al. Land use/land cover changes and climate: Modeling analysis and observational evidence. *Wiley Interdiscip. Rev. Clim. Chang.* **2011**, *2*, 828–850. [CrossRef]
5. Mahmood, R.; Pielke, R.; Hubbard, K.; Niyogi, D.; Dirmeyer, P.A.; McAlpine, C.; Carleton, A.M.; Hale, R.; Gameda, S.; Beltrán-Przekurat, A.; et al. Land cover changes and their biogeophysical effects on climate. *Int. J. Climatol.* **2014**, *34*, 929–953. [CrossRef]
6. He, J.; Yu, L.; Liu, N.; Zhao, S. Impacts of uncertainty in land surface information on simulated surface temperature and precipitation over China. *Int. J. Climatol.* **2017**, *37*, 829–847. [CrossRef]
7. Hale, R.; Gallo, K.; Loveland, T. Influences of specific land use/land cover conversions on climatological normals of near surface temperature. *J. Geophys. Res.* **2008**. [CrossRef]
8. Tao, Z.; Santanello, J.; Chin, M.; Zhou, S.; Tan, Q.; Kemp, E.; Peters-Lidard, C. Effect of land cover on atmospheric processes and air quality over the continental United States-a NASA unified WRF (NU-WRF) model study. *Atmos. Chem. Phys.* **2013**, *13*, 6207–6226. [CrossRef]
9. Teklay, A.; Dile, Y.; Asfaw, D.; Bayabil, H.; Sisay, K. Impacts of land surface model and land use data on WRF model simulations of rainfall and temperature over Lake Tana Basin, Ethiopia. *Heliyon* **2019**, *5*, e02469. [CrossRef]
10. Van Asselen, S.; Verburg, P. Land cover change or land-use intensification: Simulating land system change with a global-scale land change model. *Glob. Chang. Biol.* **2013**, *19*. [CrossRef]
11. Li, J.; Zheng, X.; Zhang, C.; Chen, Y. Impact of land-use and land-cover change on meteorology in the Beijing–Tianjin–Hebei Region from 1990 to 2010. *Sustainability* **2018**, *10*, 176. [CrossRef]
12. De Meij, A.; Vinuesa, J. Impact of SRTM and Corine Land Cover data on meteorological parameters using WRF. *Atmos. Res.* **2014**, *143*, 351–370. [CrossRef]
13. Lai, A.; Liu, Y.; Chen, X.; Chang, M.; Fan, Q.; Chan, P.; Wang, X.; Dai, J. Impact of land-use change on atmospheric environment using refined land surface properties in the Pearl River Delta, China. *Adv. Meteorol.* **2016**. [CrossRef]
14. Kirthiga, S.; Patel, N. Impact of updating land surface data on micrometeorological weather simulations from the WRF model. *Atmosfera* **2018**, *31*, 165–183. [CrossRef]
15. Lamptey, B.; Barron, E.; Pollard, D. Impacts of agriculture and urbanization on the climate of the Northeastern United States. *Glob. Planet. Chang.* **2005**, *49*, 203–221. [CrossRef]
16. Pielke, R. *Mesoscale Meteorological Modeling*, 3rd ed.; Academic Press: New York, NY, USA, 2013.
17. Shamsipour, A.; Azizi, G.; Ahmadabad, M.; Moghbel, M. Surface temperature pattern of asphalt, soil and grass in different weather condition. *J. Biodivers. Environ. Sci.* **2013**, *3*, 80–89.
18. Chudnovsky, A.; Ben-Dor, E.; Saaroni, H. Diurnal thermal behavior of selected urban objects using remote sensing measurements. *Energy Build.* **2004**, *36*, 1063–1074. [CrossRef]
19. Trusilova, K.; Jung, M.; Churkina, G.; Karsten, U.; Heimann, M.; Claussen, M. Urbanization impacts on the climate in Europe: Numerical experiments by the PSU-NCAR mesoscale model (MM5). *J. Appl. Meteorol. Climatol.* **2008**, *47*, 1442–1455. [CrossRef]
20. Mote, T.; Lacke, M.; Shepherd, J. Radar signatures of the urban effect on precipitation distribution: A case study for Atlanta, Georgia. *Geophys Res. Lett.* **2007**. [CrossRef]
21. Lei, M.; Niyogi, D.; Kishtawa, C.; Pielke, R.; Beltrán-Przekurat, A.; Nobis, T.; Vaidya, S. Effect of explicit urban land surface representation on the simulation of the 26 July 2005 heavy rain event over Mumbai, India. *Atmos. Chem. Phys.* **2008**, *8*, 5975–5995. [CrossRef]
22. Kishtawal, C.; Niyogi, D.; Tewari, M.; Pielke, R.; Shepherd, J. Urbanization signature in the observed heavy rainfall climatology over India. *Int. J. Climatol.* **2010**, *30*, 1908–1916. [CrossRef]

23. Niyogi, D.; Pyle, P.; Lei, M.; Arya, S.; Kishtawal, C.; Shepherd, M.; Chen, F.; Wolfe, B. Urban modification of thunderstorms: An observational storm climatology and model case study for the Indianapolis urban region. *J. Appl. Meteorol. Climatol.* **2011**, *50*, 1129–1144. [CrossRef]
24. Mitram, C.; Shepherd, J.; Jordan, T. On the relationship between the premonsoonal rainfall climatology and urban land cover dynamics in Kolkata city, India. *Int. J. Climatol.* **2012**, *32*, 1443–1454. [CrossRef]
25. Mas, J.; Velázquez, A.; Díaz-Gallegos, J.; Mayorga-Saucedo, R.; Alcántara, C.; Bocco, G.; Castro, R.; Fernández, T.; Pérez-Vega, A. Assessing land use/cover changes: A nationwide multidate spatial database for Mexico. *Int. J. Appl. Earth Obs.* **2004**, *5*, 249–261. [CrossRef]
26. Jáuregui, E. Effects of revegetation and new artificial water bodies on the climate of northeast Mexico City. *Energy Build.* **1990**, *15*, 447–455. [CrossRef]
27. Jáuregui, E.; Romales, E. Urban effects on convective precipitation in Mexico City. *Atmos. Environ.* **1996**, *30*, 3383–3389. [CrossRef]
28. Jazcilevich, A.; Fuentes, V.; Jáuregui, E.; Luna, E. Simulated urban climate response to historical land use modification in the basin of Mexico. *Clim. Chang.* **2000**, *44*, 515–536. [CrossRef]
29. López-Espinoza, E.; Zavala-Hidalgo, J.; Gómez-Ramos, O. Weather forecast sensitivity to changes in urban land covers using the WRF model for central Mexico. *Atmosfera* **2012**, *25*, 127–154.
30. Ochoa, C.; Quintanar, A.; Raga, G.; Baumgardner, D. Changes in intense precipitation events in Mexico City. *J. Hydrometeorol.* **2015**, *16*, 1804–1820. [CrossRef]
31. López-Bravo, C.; Caetano, E.; Magaña, V. Forecasting summertime surface temperature and precipitation in the Mexico City metropolitan area: Sensitivity of the WRF model to land cover changes. *Front. Earth Sci.* **2018**. [CrossRef]
32. Lozano-García, M.; Ortega-Guerrero, B.; Caballero-Miranda, M.; Urrutia-Fucugauchi, J. Late Pleistocene and Holocene paleoenvironments of Chalco lake, central Mexico. *Quat. Res.* **1993**, *40*, 332–342. [CrossRef]
33. Loveland, T.; Reed, B.; Brown, J.; Ohlen, D.; Zhu, Z.; Yang, L.; Merchant, J. Development of a global land cover characteristics database and IGBP DISCover from 1 km AVHRR data. *Int. J. Remote Sens.* **2000**, *21*, 1303–1330. [CrossRef]
34. Colditz, R.; López-Saldaña, G.; Maeda, P.; Argumedo-Espinoza, J.; Meneses-Tovar, C.; Victoria-Hérnandez, A.; Zermeño-Benítez, C.; Cruz-López, I.; Ressl, R. Generation and analysis of the 2005 land cover map for Mexico using 250m MODIS data. *Remote Sens. Environ.* **2012**, *123*, 541–552. [CrossRef]
35. Kain, J. The Kain–Fritsch convective parameterization: An update. *J. Appl. Meteorol.* **2004**, *43*, 170–181. [CrossRef]
36. A Description of the Advanced Research WRF Version 3. NCAR Technical Note NCAR/TN-475+STR. National Center for Atmospheric Research. Available online: https://doi:10.5065/D68S4MVH (accessed on 3 September 2020).
37. A Multi-Layer Soil Temperature Model for MM5. Available online: https://www.researchgate.net/publication/259865197_A_Multilayer_Soil_Temperature_Model_for_MM5 (accessed on 3 September 2020).
38. Zeng, X.; Wang, N.; Wang, Y.; Zheng, Y.; Zhou, Z.; Wang, G.; Chen, C.; Liu, H. WRF-simulated sensitivity to land surface schemes in short and medium ranges for a high-temperature event in East China: A comparative study. *J. Adv. Model Earth Syst.* **2015**, *7*, 1305–1325. [CrossRef]
39. Lee, C.; Kim, J.; Belorid, M.; Zhao, P. Performance evaluation of four different land surface models in WRF. *Asian J. Atmos. Environ.* **2016**, *10*, 42–50. [CrossRef]
40. Jain, S.; Panda, J.; Rath, S.; Devara, P. Evaluating land surface models in WRF simulations over DMIC region. *Indian J. Sci. Technol.* **2017**, *10*, 1–24. [CrossRef]
41. Wilks, D. *Statistical Methods in the Atmospheric Sciences*, 3rd ed.; Academic Press: San Diego, CA, USA, 2011.
42. American Geophysical Union. Comparison and Evaluation of Five Global Land Cover Datasets for Mexico. Spring Meeting 2013 Abstract Id. A23A-02. Available online: https://ui.adsabs.harvard.edu/abs/2013AGUSM.A23A..02L/abstract (accessed on 3 September 2020).
43. Yang, H.; Li, S.; Chen, J.; Zhang, X.; Xu, S. The standardization and harmonization of land cover classification systems towards harmonized datasets: A review. *ISPRS Int. J. Geo-Inf.* **2017**, *6*, 154. [CrossRef]
44. Colditz, R.; Llamas, R.; Ressl, R. Detecting Change Areas in Mexico Between 2005 and 2010 Using 250 m MODIS Images. *IEEE J. Select Top Appl. Earth Obs. Remote Sens.* **2014**, *7*, 3358–3372. [CrossRef]
45. Barrales-Hassan, R. Impacto del Cambio de Uso de Suelo y Cobertura Vegetal en el Pronóstico Numérico del Tiempo. Bachelor's Thesis, Universidad Nacional Autónoma de México, Mexico City, Mexico, 2017.

46. A Land Use and Land Cover Classification System for Use with Remote Sensor Data. 1st ed. United States Geological Survey. Available online: https://pubs.usgs.gov/pp/0964/report.pdf (accessed on 3 September 2020).
47. Bai, L. *Comparison and Validation of Five Land Cover Products over the AFRICAN Continent*; Lund University: Lund, Sweden, 2010.
48. Latifovic, R.; Zhu, Z.; Cihlar, J.; Giri, C.; Olthof, I. Land cover mapping of North and Central America-global land cover 2000. *Remote Sens. Environ.* **2004**, *89*, 116–127. [CrossRef]
49. McCallum, I.; Obersteiner, M.; Nilsson, S.; Shvidenko, A. A spatial comparison of four satellite derived 1 km global land cover datasets. *Int. J. Appl. Earth Obs.* **2006**, *8*, 246–255. [CrossRef]
50. Zhou, L.; Dickinson, R.; Tian, Y.; Fang, J.; Li, Q.; Kaufmann, R.; Tucker, C.; Myneni, R. Evidence for a significant urbanization effect on climate in China. *Proc. Natl. Acad. Sci. USA* **2004**, *101*, 9540–9544. [CrossRef] [PubMed]
51. Jin, J.; Miller, N.; Schlegel, N. Sensitivity study of four land surface schemes in the WRF model. *Adv. Meteorol.* **2010**. [CrossRef]